ACS APPLIED MATERIALS & INTERFACES

www.acsami.org

Research Article

Rational Engineering of the DNA Walker Amplification Strategy by Using a Au@Ti_3C_2@PEI-Ru(dcbpy)$_3^{2+}$ Nanocomposite Biosensor for Detection of the SARS-CoV-2 RdRp Gene

Bo Yao,[§] Jing Zhang,[§] Zhenqiang Fan, Yuedi Ding, Bin Zhou, Runlin Yang, Jianfeng Zhao,* and Kai Zhang*

Cite This: *ACS Appl. Mater. Interfaces* 2021, 13, 19816−19824

Read Online

ACCESS | Metrics & More | Article Recommendations | Supporting Information

ABSTRACT: The detection of the severe acute respiratory syndrome coronavirus 2 (SARS-CoV-2) is crucial for preventing and controlling infectious diseases and disease treatment. In this work, a Au@Ti_3C_2@PEI-Ru(dcbpy)$_3^{2+}$ nanocomposite-based electrochemiluminescence (ECL) biosensor was rationally designed, which realized sensitive detection of the RNA-dependent RNA polymerase (RdRp) gene of SARS-CoV-2. In addition, a DNA walker was also used to excise the hairpin DNAs under the action of Nb.BbvCI endonuclease. Furthermore, model DNA−Ag nanoclusters (model DNA−AgNCs) were used to quench the initial ECL signal. As a result, the ECL biosensor was used to sensitively detect the SARS-CoV-2 RdRp gene with a detection range of 1 fM to 100 pM and a limit of detection of 0.21 fM. It was indicated that the ECL biosensor had a great application potential for clinical medical detection. Furthermore, the DNA walker amplification also played a reliable candidate strategy for other detection methods.

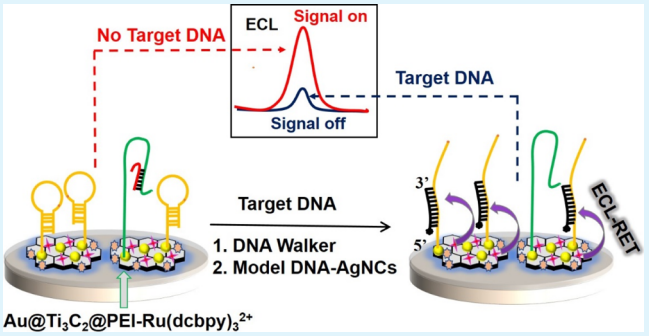

KEYWORDS: *SARS-CoV-2, RNA-dependent RNA polymerase, MXene-Ti_3C_2, DNA walker, electrochemiluminescence, biosensor*

INTRODUCTION

At the end of 2019, severe acute respiratory syndrome coronavirus 2 (SARS-CoV-2) endangered the physical and mental health of humans all over the world.[1] The rapid transmission speed and strong infectious capacity of SARS-CoV-2 have led to a large increase of infected people every day.[2] However, there are still no specific drugs and effective targeted therapy developed. Therefore, the early detection of SARS-CoV-2 is essential to human lives, health, and safety. The early clinical diagnosis of SARS-CoV-2 is really a great challenge due to the similar symptoms as other respiratory diseases, including cough and fever.[3] Therefore, it becomes urgent and significant for the timely and accurate laboratory diagnosis of SARS-CoV-2.[4] Reported detection of different regions of the SARS-CoV-2 genome included the nucleocapsid protein gene (N gene), envelope protein gene (E gene), spike protein gene (S gene), and RNA-dependent RNA polymerase gene (RdRp gene) by using the real-time reverse transcriptase polymerase chain reaction (RT-PCR).[5] Detection of different regions of the SARS-CoV-2 genome will affect the specificity and accuracy of the assay. The N gene may cross-react with other coronaviruses and has a low sensitivity (8.3 copies per reaction).[6] The S gene is the most variable region in the genome.[7] The E gene is a conserved region throughout the beta-coronavirus and can be distinguished from other viruses but not from severe acute respiratory syndrome (SARS-CoV, the outbreak began in 2002/2003) and SARS-CoV-2.[8] The RdRp gene located in ORF1ab region possesses strong specificity and high sensitivity (3.6 copies per reaction), which can distinguish SARS-CoV-2 from SARS-CoV.[9,10] The widespread use of the RdRp gene as a target for detection in Europe has shown outstanding performance.[11] Therefore, the detection of the RdRp gene for SARS-CoV-2 is of unparalleled significance. Currently, RT-PCR-based diagnosis of SARS-CoV-2 in hospitals and laboratories around the world is the current gold standard.[12] Corman et al. reported a method for detecting the SARS-CoV-2 RdRp gene using RT-PCR.[13] However, there are still disadvantages of RT-PCR, including expensive equipment, easy degradation of RNA, and complicated operation steps to detect SARS-CoV-2.[2] There-

Received: March 9, 2021
Accepted: April 13, 2021
Published: April 23, 2021

https://doi.org/10.1021/acsami.1c04453
ACS Appl. Mater. Interfaces 2021, 13, 19816−19824

fore, it is urgent to find a fast, efficient, portable, and simple detection method.

Among various detection methods, electrochemiluminescence (ECL) technology has been extensively applied, thanks to the advantages, including simple operation, inexpensive instrument, high sensitivity, and low background noise.[14−17] In order to further improve the performance of ECL biosensors, two-dimensional (2D) nanomaterials were introduced into the ECL system. As a new type of 2D transition-metal compound with lots of merits, including large specific surface area, excellent hydrophilicity, strong reduction ability, good biocompatibility, environment-friendly nature, and high stability, the ascendant MXene nanomaterials have attracted widespread attention. Many members of MXenes have been reported, including Ti_3C_2, Ti_2C, Ti_2N, Nb_2C, V_2C, and so on.[18] Among them, Ti_3C_2 terminated with OH^- has a metallic conductivity up to 6500 S cm^{-1} and has excellent potential as an electrode material.[19,20] The introduction of MXenes in the construction of biosensors is a good strategy since ultrathin MXenes can easily modify signal molecules or nanoparticles.[21] Zhang et al. reported the detection of exosomes via MXene nanosheets with enhanced ECL signals in the luminol system.[22] Therefore, MXene-based nanomaterials would be a powerful tool to broaden the research field and improve much more advanced performance of ECL biosensors.

A DNA walker can improve detection sensitivity, reduce detection limit, accelerate signal amplification, and shorten detection time in biosensors.[23,24] Furthermore, the DNA walker can amplify the signal by providing energy to drive the walking chain moving along a specific track.[25] Its full advantages cover strong flexibility, controllability, automation, and mobile stability.[26] During the process of walking, multiple substrates are released as enzyme-cleavage products. In general, the DNA walker is generally divided into unipedal DNA walker,[27] bipedal DNA walker,[28] and multipedal DNA walker[29] based on the number of walking feet. Compared with the bipedal and multipedal DNA walker, the unipedal DNA walker is widely used in circular amplification systems without dissociation from the track. Therefore, it is necessary to introduce a unipedal, enzyme-driven DNA walker in biosensors.

Inspired by that, the detection of the RdRp gene as the target can effectively distinguish SARS-CoV and SARS-CoV-2 with high sensitivity. We constructed a sensitive ECL biosensor based on the Au@Ti_3C_2@PEI-Ru(dcbpy)$_3^{2+}$ nanocomposites to detect the SARS-CoV-2 RdRp gene. Among the Au@Ti_3C_2@PEI-Ru(dcbpy)$_3^{2+}$ nanocomposites, MXene-Ti_3C_2 not only possessed good electrical conductivity but also had a large specific surface area, which could uniformly disperse Au nanoparticles (Au NPs) and loaded a large amount Ru(dcbpy)$_3^{2+}$. In addition, polyethylenimine (PEI) as a coreactant could improve the luminous efficiency of Ru(dcbpy)$_3^{2+}$. Based on these advantages, Au@Ti_3C_2@PEI-Ru(dcbpy)$_3^{2+}$ obtained excellent ECL performance, can improve the sensitivity of biosensor, and can be used as an excellent bioanalytical material. Furthermore, under the action of energy provided by Nb.BbvCI, numerous hairpin DNAs (HP DNAs) were excised by the amplification strategy of the unipedal DNA walker. Eventually, model DNA−Ag nanoclusters (model DNA−AgNCs) were used to quench the ECL signal. As a result, the novel ECL biosensor achieved a limit of detection (LOD) of 0.21 fM for the detection of the RdRp gene, which would exhibit great significance in the clinical detection in medicine.

EXPERIMENTAL SECTION

Materials and Reagents. Chloroauric acid ($HAuCl_4$), PEI, Nafion 117 solution (5%), 1-ethyl-3-(3-dimethyllaminopropyl)-carbodiimide hydrochloride (EDC), and *N*-hydroxysuccinimide (NHS) were obtained from Aladdin Biochemical Technology Co. Ltd. (Shanghai, China). MXene-Ti_3C_2 (5 mg mL^{-1}, few-layer Ti_3C_2 dispersion) was obtained from Nanjing Xianfeng Nano Co. Ltd. (Nanjing, China). Tris(2-carboxyethyl) phosphine hydrochloride (TCEP) and 6-mercaptohexanol (MCH) were obtained from Sigma-Aldrich (St Louis, MO, USA). Silver nitrate ($AgNO_3$) and sodium borohydride ($NaBH_4$) were purchased from Sinopharm Chemical Reagent Co. Ltd. (Shanghai, China). Tris(4,4′-dicarboxylicacid-2,2′-bipyridyl)ruthenium(II) dichloride (Ru(dcbpy)$_3^{2+}$) was purchased from Suna Tech Inc. (Suzhou, China). Tris-(hydroxymethyl)aminomethane hydrochloride (Tris-HCl) and phosphate buffer solution (PBS) were purchased from Sangon Biotech Co. Ltd. (Shanghai, China). Nb.BbvCI enzyme and 10× NEB buffer were purchased from New England Biolabs (USA). Modified oligonucleotides were synthesized by Genscript Biotechnology Co. Ltd. (Nanjing, China), and the sequence of oligonucleotides is depicted in Table S1.

Apparatus. Various morphologies of nanomaterials were characterized by scanning electron microscopy (Sigma 500, Carl Zeiss, Germany) and field-emission transmission electron microscopy (TEM) (JEM-2100 F, JEOL, Japan). Fourier transform infrared (FT-IR) spectra were characterized by a PerkinElmer Spectrum GX spectrometer (PerkinElmer Co., Waltham, MA). Electrochemical impedance spectroscopy (EIS) and cyclic voltammetry (CV) were measured by an electrochemical workstation (CHI660E, Shanghai Chenhua Instrument Co., Ltd, Shanghai, China). The ECL signal was captured by ECL-6B belonging to the State Key Laboratory of Analytical Chemistry for Life Sciences, Nanjing University. A three-electrode system was applied with a platinum (Pt) wire electrode as the counter electrode, Ag/AgCl electrode as the reference electrode, and 3 mm-diameter modified glassy carbon electrode (GCE) as the working electrode. Electrophoretic image was taken by a ChemiDoc MP Imager (Bio-Rad, USA).

Synthesis of Au@Ti_3C_2@PEI-Ru(dcbpy)$_3^{2+}$ Nanocomposites. The Au@Ti_3C_2@PEI-Ru(dcbpy)$_3^{2+}$ nanocomposites were successfully synthesized through the $NaBH_4$ reduction method according to the previous literature.[18,22,30] First of all, 10 mg of Ru(dcbpy)$_3^{2+}$ powder was dissolved in 4 mL of PBS (0.1 M, pH = 7.4). Second, EDC (400 mM)/NHS (100 mM) mixed solution was added to the above solution and kept stirring in room temperature for 2 h. At the same time, 1 mL of Ti_3C_2 solution (5 mg mL^{-1}) mixed with 5 mL of PEI solution (1% w/v). Third, all the Ti_3C_2 and PEI mixed solution were added to the Ru(dcbpy)$_3^{2+}$ of PBS and continuously agitated for 2 h. In this way, Ru(dcbpy)$_3^{2+}$ and PEI are combined together firmly by the amide bond. Fourth, 400 μL of $HAuCl_4$ (1%) and 1 mL of $NaBH_4$ (0.2 M) solution were added to the above solution continuously stirring for 1 h, and $HAuCl_4$ was reduced to Au NPs by $NaBH_4$. Finally, all the mixture was centrifuged at 12,000 rpm for 5 min, dispersed, and washed several times by ultrapure water and ethanol. The obtained Au@Ti_3C_2@PEI-Ru(dcbpy)$_3^{2+}$ nanocomposites were dispersed in 1 mL of PBS (0.1 M, pH = 7.4) and stored at 4 °C for the next assay.

Synthesis of Model DNA−AgNCs. Model DNA−AgNCs were synthesized according to a previous literature.[31] In brief, 5 μL of model DNA was dissolved in PBS (0.1 M, pH = 6), which was added with 150 μM $AgNO_3$ solution and shaken vigorously for 3 min and stewed for 1 h at room temperature. Then, 150 μM of ice-cold fresh $NaBH_4$ solution was quickly added to the above solution and shaken for 3 min. At last, the mixed solution was placed in a dark environment at 4 °C for 12 h, and a homogeneous model DNA−AgNC pale yellow solution was observed.

Nondenaturing Polyacrylamide Gel Electrophoresis. First, the electrophoresis instrument run at 80 V for 30 min. Then, 10 μL of

https://doi.org/10.1021/acsami.1c04453
ACS Appl. Mater. Interfaces 2021, 13, 19816−19824

Scheme 1. Schematic Illustration of (A) Preparation of Au@Ti_3C_2@PEI-Ru(dcbpy)$_3^{2+}$ Nanocomposites; (B) based on Au@Ti_3C_2@PEI-Ru(dcbpy)$_3^{2+}$ Nanocomposites ECL Biosensor Detection of the SARS-CoV-2 RdRp Gene Combined Unipedal DNA Walker Amplification Strategy

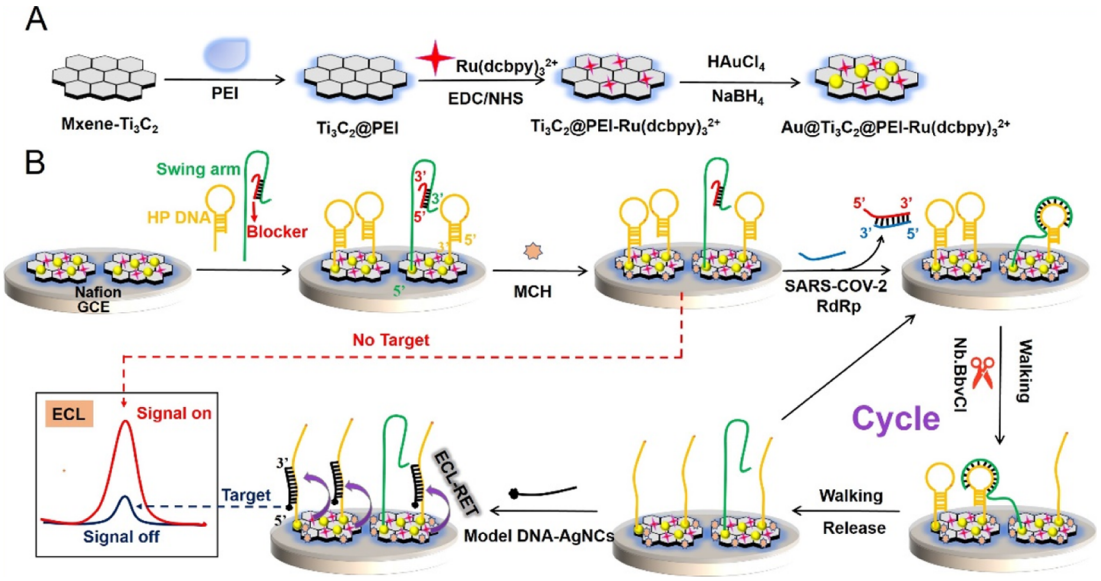

the sample was mixed with the loading buffer evenly. The mixed solution was then injected into the 20% nondenaturing polyacrylamide gel sample tank, and then, the polyacrylamide gel was run for 2 h. Third, the gel was immersed in GelRed color developing solution for 30 min. Finally, the electrophoretic image was filmed by a ChemiDoc MP Imager.

Preparation of Basal Solution. The basal solution was prepared through the following steps. First, 0.4 μM swing arm and 0.5 μM blocker were dissolved in Tris-HCl (pH = 8.0) and kept at 90 °C for 5 min to prepare a swing arm-blocker double-chain structure. Subsequently, the 8 μM HP DNAs was added to the mixed solution. Lastly, the mixed solution was treated with 10 mM TCEP for 1 h in the dark environment to cut off the S−S bond. In the end, the basal solution was obtained.

ECL Biosensor Preparation. Before modification, the GCE was carefully polished and cleaned according to the previous method.[32] First, the GCE surface was covered by 0.5% Nafion, and 10 μL of Au@Ti_3C_2@PEI-Ru(dcbpy)$_3^{2+}$ nanocomposites solution was dispersed onto the Nafion/GCE surface and dried at room temperature. Then, the modified electrode was immersed in the 200 μL basal solution for 12 h. Subsequently, 5 μL of MCH (1 mM) was dripped on the electrode surface and incubated at 37 °C for 2 h. Next, the modified electrode was immersed in a mixed solution with different concentrations of target DNA and 6 U Nb.BbvCI and incubated for 80 min. After that, the modified electrode was immersed in 200 μL of model DNA−AgNC solution for 40 min. Finally, the decorated electrode was washed several times with PBS (0.1 M, pH = 7.4) and stored in a refrigerator at 4 °C for the next assay. It is worth reminding that after each stepwise modification of the electrode, the electrode was washed with PBS (0.1 M) twice. In the end, the ECL experiment was carried out with a three-electrode system measured in PBS (0.1 M, pH = 7.4) with 0−1.3 V scanning voltage.

RESULTS AND DISCUSSION

Principle of the Assay. The synthesis process of Au@Ti_3C_2@PEI-Ru(dcbpy)$_3^{2+}$ nanocomposites is shown in Scheme 1A. The construction and detection principle of the ECL biosensor are shown in Scheme 1B. First of all, Nafion and the Au@Ti_3C_2@PEI-Ru(dcbpy)$_3^{2+}$ nanocomposites were added dropwise successively on the bare GCE. Subsequently, the HP DNAs (including a sequence "5′-GCTGAGG-3′" that could be cleaved by Nb.BbvCI) and swing arm-blocker were anchored on the Au@Ti_3C_2@PEI-Ru(dcbpy)$_3^{2+}$ nanocomposites surface via the Au−S bond, which possessed a strong ECL signal called "signal on" state. In this case, the swing arm was imprisoned by the blocker and prohibited to hybridize with HP DNAs. However, when introduced to the system, the target DNA (SARS-CoV-2 RdRp) captured the blocker to form the target DNA−blocker duplex with the help of a toehold, leading to the swing arm freedom. The free swing arm combined with the HP DNA and severed HP DNA with the help of Nb.BbvCI. Then, the swing arm was released again and combined with another HP DNA to continue severing of the HP DNA under the action of Nb.BbvCI to start the walking process. This cycling process was called walking of the DNA walker, which is used in biology as an amplification strategy. The leaving fragments of HP DNAs combined with the model DNA−AgNCs after being excised by the DNA walker. In this way, the ECL signal was quenched through ECL resonance energy transfer and can be achieved when the donor (Au@Ti_3C_2@PEI-Ru(dcbpy)$_3^{2+}$) and acceptor (model DNA−AgNCs) are close and the ECL emission spectrum of the Au@Ti_3C_2@PEI-Ru(dcbpy)$_3^{2+}$ and the UV−vis absorption spectrum of the model DNA−AgNCs overlap (shown in Figure S1), which is called the "signal off" state. Therefore, when the target DNA is presented in the system, the ECL biosensor could realize the transition from "signal on" to "signal off" state. However, when no target DNA existed in the system, the ECL biosensor could not realize the "signal off" state. Based on this model, the ECL intensity change of the ECL biosensor could reflect different target DNA concentrations.

Possible Luminescence Mechanism of the ECL Biosensor. Referring to the previous literature,[18,33] we discussed the possible luminescence mechanism of the ECL biosensor based on Au@Ti_3C_2@PEI-Ru(dcbpy)$_3^{2+}$ nanocomposites, as described in the following eqs 1−4. In order to obtain an ECL signal, initially, Ti_3C_2-Ru(II) and PEI were oxidized to Ti_3C_2-Ru(III) and PEI$^{\bullet+}$ (eq 1), respectively. Then, PEI$^{\bullet+}$ reacted to PEI$^{\bullet}$ (eq 2). Subsequently, the PEI$^{\bullet}$ reduced Ti_3C_2-Ru(III) to the excited-state Ti_3C_2-Ru(II)* (eq

https://doi.org/10.1021/acsami.1c04453
ACS Appl. Mater. Interfaces 2021, 13, 19816−19824

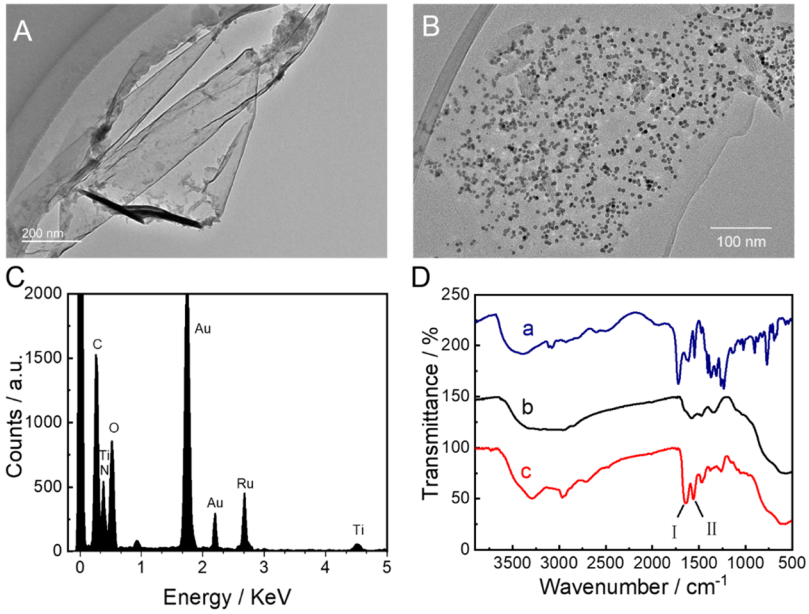

Figure 1. (A) TEM image of Ti_3C_2 nanosheets; (B) TEM image of Au@Ti_3C_2@PEI-Ru(dcbpy)$_3^{2+}$ nanocomposites; (C) EDS spectra of Au@Ti_3C_2@PEI-Ru(dcbpy)$_3^{2+}$ nanocomposites; (D) FT-IR spectra of Ru(dcbpy)$_3^{2+}$ (curve a), Au@Ti_3C_2@PEI (curve b), and Au@Ti_3C_2@PEI-Ru(dcbpy)$_3^{2+}$ nanocomposites (curve c).

3). Finally, the excited-state Ti_3C_2-Ru(II)* radiated transfer to the ground-state Ti_3C_2-Ru(II) and released photons (eq 4).

$$[Ti_3C_2\text{-Ru(II)}] + \text{PEI-2e}^- \rightarrow [Ti_3C_2\text{-Ru(III)}] + \text{PEI}^{\bullet+} \quad (1)$$

$$[Ti_3C_2\text{-Ru(III)}] + \text{PEI}^{\bullet+} \rightarrow [Ti_3C_2\text{-Ru(III)}] + \text{PEI}^{\bullet} + H^+ \quad (2)$$

$$[Ti_3C_2\text{-Ru(III)}] + \text{PEI}^{\bullet} \rightarrow [Ti_3C_2\text{-Ru(II)*}] + \text{PEI} \quad (3)$$

$$[Ti_3C_2\text{-Ru(II)*}] \rightarrow [Ti_3C_2\text{-Ru(II)}] + h\nu \quad (4)$$

Characterization of Ti_3C_2 Nanosheets, Au@Ti_3C_2@PEI-Ru(dcbpy)$_3^{2+}$ Nanocomposites, and Model DNA−AgNCs. The morphology of Ti_3C_2 nanosheets was characterized by TEM, and a graphene-like surface is observed in Figure 1A. The TEM image of the Au@Ti_3C_2@PEI-Ru(dcbpy)$_3^{2+}$ nanocomposites is shown in Figure 1B. The Au NPs were uniformly dispersed on the Ti_3C_2 surface. Figure S2 shows the high-resolution transmission electron microscopy (HRTEM) image of Au NPs with the size of 4−8 nm. Figures 1C and 2 are EDS spectra and elemental mapping analyses. It was proved that Ti, C, N, Ru, and Au elements typically existed in Au@Ti_3C_2@PEI-Ru(dcbpy)$_3^{2+}$ nanocomposites. As seen in Figure 1D, the FT-IR spectrum of Au@Ti_3C_2@PEI (curve b) showed a large broad peak at 3100−3500 cm^{-1} for the N−H stretching vibration of amino groups. The next interaction with Ru(dcbpy)$_3^{2+}$ (curve a) resulted in Au@Ti_3C_2@PEI-Ru(dcbpy)$_3^{2+}$ nanocomposites. The FT-IR spectra of Au@Ti_3C_2@PEI-Ru(dcbpy)$_3^{2+}$ nanocomposites (curve c) showed characteristic amide vibrations with the C═O stretching vibration at 1634 cm^{-1} (amide I) and N−H bending/C−N stretching at 1559 cm^{-1} (amide II), indicating that the Au@Ti_3C_2@PEI-Ru(dcbpy)$_3^{2+}$ nanocomposites were successfully fabricated by the amide reaction. This result further confirmed that the Au@Ti_3C_2@PEI-Ru(dcbpy)$_3^{2+}$ nanocomposites were successfully synthesized. Furthermore, the stability of Au@Ti_3C_2@PEI-Ru(dcbpy)$_3^{2+}$ nanocomposites modified on the GCE is demonstrated in Figure S3. The HRTEM image of model DNA−AgNCs is shown in Figure S4, which shows that the diameter of model DNA−AgNCs was 4−6 nm.

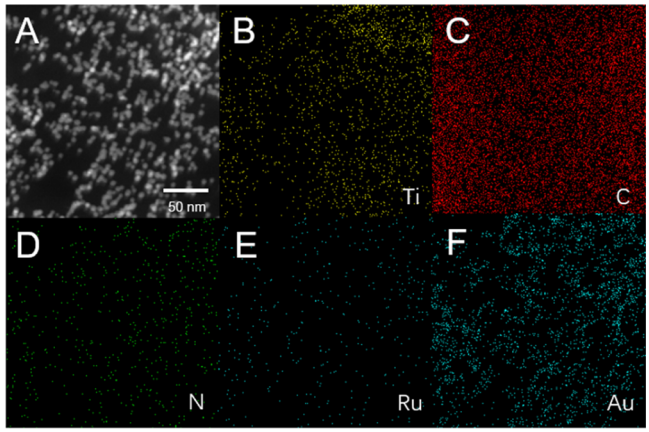

Figure 2. Elemental mapping analyses of Au@Ti_3C_2@PEI-Ru(dcbpy)$_3^{2+}$ nanocomposites; Ti (B), C (C), N (D), Ru (E), and Au (F) elements.

Feasibility of the ECL Biosensor. CV, EIS, ECL, and polyacrylamide gel electrophoresis (PAGE) analysis were used to characterize the construction process of the biosensor, as described in Figure 3. As shown in Figure 3A, CV was used to monitor the construction process of the biosensor and measured in 5 mM $[Fe(CN)_6]^{3-/4-}$ solution. When a bare electrode (curve a) existed, there was the largest redox peak. While Nafion was modified on the electrode (curve b), the redox peak current decreased to the bottom due to the poor conductivity of the Nafion polymer. The Au@Ti_3C_2@PEI-Ru(dcbpy)$_3^{2+}$ nanocomposites (curve c) were modified on the electrode and the redox peak current significantly increased due to the excellent conductivity of Ti_3C_2 and Au NPs. Subsequently, the swing arm-blocker + HP DNAs (curve d)

https://doi.org/10.1021/acsami.1c04453
ACS Appl. Mater. Interfaces 2021, 13, 19816−19824

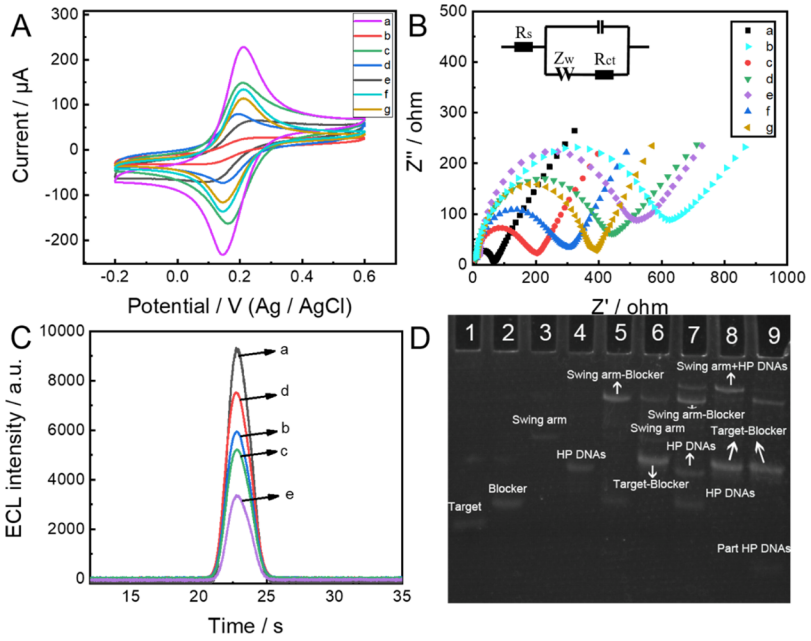

Figure 3. Characterization of stepwise incubation of the biosensor for (A) CV, (B) EIS, (C) ECL, and (D) PAGE analysis. (A) CV and (B) ECL curves of (a) GCE, (b) Nafion/GCE, (c) Au@Ti_3C_2@PEI-Ru(dcbpy)$_3^{2+}$/Nafion/GCE, (d) HP DNAs, swing arm-blocker/Au@Ti_3C_2@PEI-Ru(dcbpy)$_3^{2+}$/Nafion/GCE, (e) MCH/HP DNAs, swing arm-blocker/Au@Ti_3C_2@PEI-Ru(dcbpy)$_3^{2+}$/Nafion/GCE, (f) incubation with the reaction solution consisting of target DNA and Nb.BbvCI, (g) next treatment with the model DNA−AgNCs; (C) ECL-time curves of (a) Au@Ti_3C_2@PEI-Ru(dcbpy)$_3^{2+}$/Nafion/GCE, (b) HP DNAs, swing arm-blocker/Au@Ti_3C_2@PEI-Ru(dcbpy)$_3^{2+}$/Nafion/GCE, (c) MCH/HP DNAs, swing arm-blocker/Au@Ti_3C_2@PEI-Ru(dcbpy)$_3^{2+}$/Nafion/GCE, (d) incubation with the reaction solution consisting of target DNA and Nb.BbvCI, (e) next treatment with the model DNA−AgNCs; (D) PAGE analysis of different samples. Lane 1: target DNA, lane 2: blocker, lane 3: swing arm, lane 4: HP DNAs, lane 5: swing arm-blocker, lane 6: swing arm-blocker + target DNA, lane 7: swing arm-blocker + HP DNAs, lane 8: swing arm-blocker + HP DNAs + target DNA, lane 9: swing arm-blocker + HP DNAs were treated with target DNA and Nb.BbvCI.

and MCH (curve e) were modified on the surface of the electrode, followed by the decreased peak current. After incubating with the target DNA and Nb.BbvCI (curve f), the swing arm was released. Then, lots of HP DNAs were excised, leading to the increased redox peak current. Finally, when the model DNA−AgNCs (curve g) were incubated on the electrode surface, the peak current dropped down. It was indicated that the biosensor was successfully constructed.

As shown in Figure 3B, EIS was also used to characterize the construction process of the biosensor. Moreover, the experiment was performed in 5 mM $[Fe(CN)_6]^{3-/4-}$ solution. Above all, the impedance of the bare electrode turned into the smallest (curve a). After being modified with Nafion (curve b), the impedance became the largest. Also, when the electrode was coated with the Au@Ti_3C_2@PEI-Ru(dcbpy)$_3^{2+}$ nanocomposites (curve c), the impedance decreased. Thereafter, the swing arm-blocker + HP DNAs (curve d) were modified onto the electrode, and the increased impedance implied that HP DNAs, swing arm-blocker and Au NPs were linked together through the Au−S bonds. When the nonconductive material MCH (curve e) was modified on the electrode surface, the impedance increased. After incubating with the target DNA and Nb.BbvCI (curve f) to the electrode surface, the impedance reduced. In the end, model DNA−AgNCs (curve g) were added to the modified electrode surface with increased impedance. The EIS results also indicated that the biosensor was successfully constructed.

Figure 3C demonstrates the ECL signal intensity of the biosensor construction process. The experiment was executed in PBS (0.1 M, pH = 7.4). When the GCE/Nafion was modified with Au@Ti_3C_2@PEI-Ru(dcbpy)$_3^{2+}$ nanocomposites (curve a), the strongest signal showed up. Subsequently, the swing arm-blocker + HP DNAs (curve b), and MCH (curve c) were sequentially modified onto the electrode, and the ECL signal intensity decreased successively. When the electrode was incubated with the target DNA and Nb.BbvCI (curve d), the ECL signal intensity increased. Finally, the model DNA−AgNCs (curve e) were incubated on the electrode, and the ECL signal was quenched. These results were consistent with CV and EIS data, demonstrating the feasibility of biosensor design.

Besides, according to gel electrophoresis, the feasibility of the DNA walker was also confirmed in Figure 3D. When the blocker (lane 2) and swing arm (lane 3) were mixed with each other, a new band (lane 5) was generated due to the formation of a swing arm-blocker double-stranded structure. When target DNA (lane 1) was introduced, a new band formed (lane 6), which was due to target DNA displacing the blocker to form target DNA−blocker double strands. Subsequently, HP DNAs and the swing arm-blocker were mixed together (lane 7) and target DNA was introduced, which can be seen to form a target DNA-blocker double-stranded and swing arm-HP DNA hybrid structure (lane 8). When Nb.BbvCI was continuously introduced, HP DNA was excised and observed at the bottom of lane 9. Thus, it was demonstrated that the DNA walker was completed.

Optimization of Analytical Conditions. To achieve the excellent performance of the biosensor, the incubation time of the target DNA and Nb.BbvCI, the concentration of model DNA−AgNCs, the concentration ratio of swing arm-blocker to HP DNAs in the basal solution, and the dosage of Nb.BbvCI were optimized. Figure 4A shows the change curves of the

https://doi.org/10.1021/acsami.1c04453
ACS Appl. Mater. Interfaces 2021, 13, 19816−19824

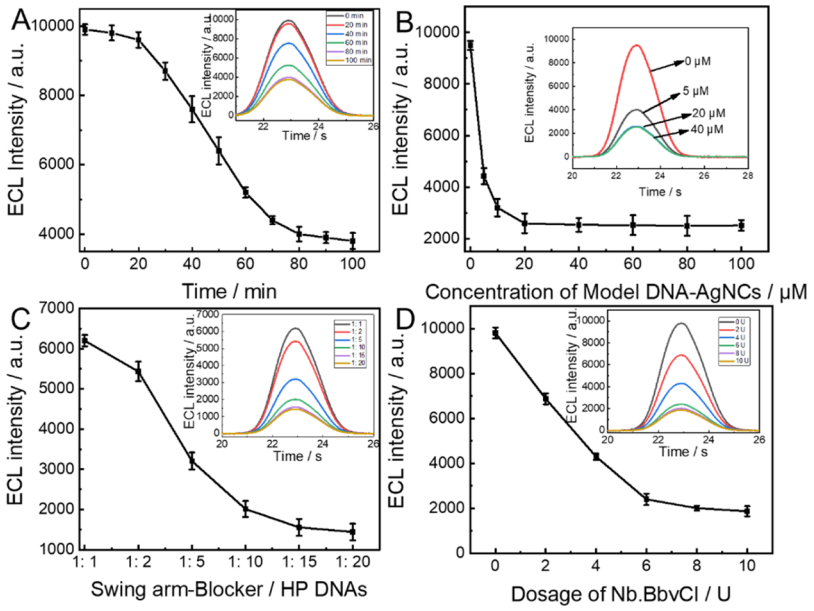

Figure 4. Choosing appropriate experimental parameters for the ECL biosensor: (A) incubation time curves of mixed target DNA and Nb.BbvCI; (B) concentration of model DNA−AgNCs; (C) concentration ratio of the swing arm-blocker to HP DNAs; (D) dosage of Nb.BbvCI on the ECL signal intensity.

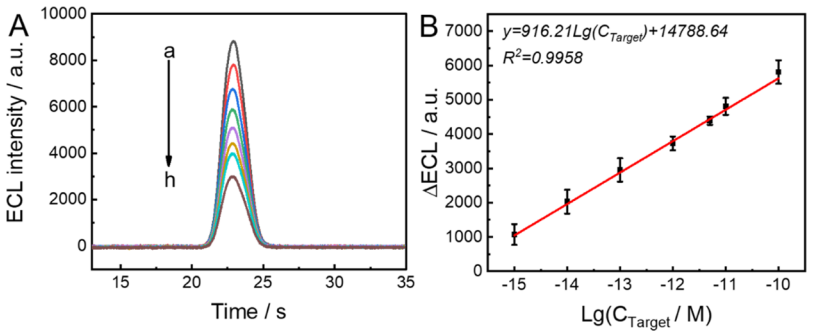

Figure 5. (A) Time density curves of ECL with different concentrations of target DNA in 0.1 M PBS (the concentrations of target DNA from a to h were 0 fM, 1 fM, 10 fM, 100 fM, 1 pM, 5 pM, 10 pM, and 100 pM); (B) calibration curves of the logarithm of target DNA concentration and ECL density.

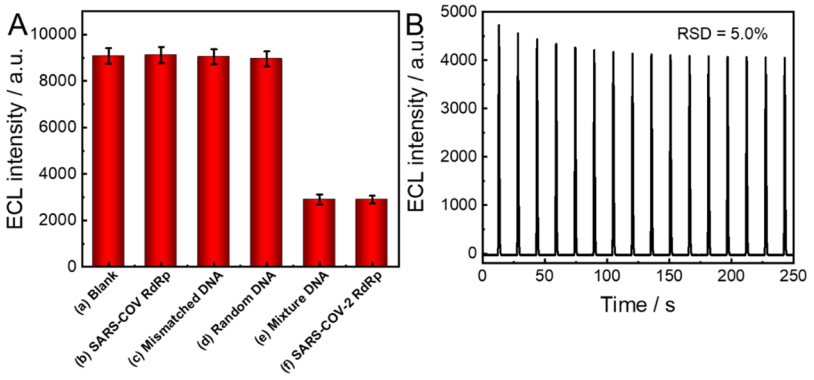

Figure 6. (A) Specificity of the ECL biosensor for different DNAs: (a) blank solution, (b) 1 nM RdRp gene of SARS-CoV, (c) 1 nM mismatched DNA, (d) 1 nM random DNA, (e) mixture DNA, including 1 nM SARS-CoV RdRp gene, 100 pM SARS-CoV-2 RdRp gene, 1 nM random DNA and 1 nM mismatched DNA, (f) 100 pM RdRp-SARS-CoV-2; (B) stability of the ECL biosensor.

ECL signal intensity with the increased incubation time of target DNA and Nb.BbvCI. The ECL signal intensity gradually decreased and finally stabilized at 80 min, which was also regarded as the optimal incubation time for the target DNA and Nb.BbvCI. The concentration of model DNA−AgNCs was equally essential for the performance of the biosensor, as shown in Figure 4B. The ECL signal intensity reached a plateau after 20 μM, reflecting that the model DNA−AgNCs effectively quenched the ECL signal, with the appropriate concentration for model DNA−AgNCs being 20 μM. In

https://doi.org/10.1021/acsami.1c04453
ACS Appl. Mater. Interfaces 2021, 13, 19816−19824

Figure 4C, the swing arm-blocker and HP DNAs in basal solution were cultivated on the electrode surface simultaneously, and the effect of the concentration ratio on the ECL signal intensity was studied. The optimal ratio of swing-arm blocker to HP DNAs was 1:20 in the basal solution. Figure 4D reveals the change in the ECL signal intensity as the dosage of Nb.BbvCI increased. When the dosage of Nb.BbvCI reached 6 U, the trend of the ECL signal intensity became stable. As a result, 6 U of Nb.BbvCI was selected as the optimal dosage in this experiment.

Analytical Performance of the ECL Biosensor. The sensitivity of the ECL biosensor was detected under optimal conditions when the target DNA at different concentrations was presented in the system. As shown in Figure 5A, as the target DNA concentration increased from 1 fM to 100 pM, the ECL signal intensity gradually decreased. As shown in Figure 5B, the logarithm of the target DNA concentration from 1 fM to 100 pM possessed an excellent linear relationship with the signal intensity of ECL, and the linear regression equation was $y = 916.21 \lg(C_{target}(\mathrm{mol})) + 14788.64$ ($R^2 = 0.9958$). The LOD is based on the formula LOD = $3\sigma/k$, where σ represents the standard deviation of the blank sample, and k represents the slope of the regression equation. The LOD of the proposed biosensor was calculated as 0.21 fM. Various detection methods are shown in Table S2. Compared with other methods of detecting the SARS-CoV-2, our method still exhibited a low LOD.

Specificity and Stability of the ECL Biosensor. Specificity and stability are essential indicators for evaluating the ECL biosensor. Therefore, various interferences including the RdRp gene of SARS-CoV (1 nM), mismatched DNA (1 nM), random DNA (1 nM) were imported to evaluate the specificity of the biosensor and are shown in Figure 6A. When these interferences were presented in the system, the biosensor exhibited an extreme ECL signal intensity similar to the blank (the relevant nucleic acid sequence is described in Table S1). Among them, the RdRp gene of SARS-CoV was similar to the RdRp gene of SARS-CoV-2 (100 pM). However, it still had a good discrimination degree according to the ECL signal intensity. Moreover, the biosensor was able to detect the SARS-CoV-2 RdRp gene in the mixture DNA, ascribed to the better selectivity of the biosensor. At 5 pM of target DNA (Figure 6B), the biosensor was tested for 16 continuous cycles with minimally decreased ECL intensity and 5.0% relative standard deviation (RSD), indicating its high stability.

Real Sample Analysis in Human Serum. To examine the potential application of the ECL biosensor for clinical medicine, a standard addition method was used to detect different concentrations of target DNA in human serum for recovery experiments. Different concentrations of target DNA were added to 10-fold diluted human serum. As described in Table S3, the experimental recoveries ranged from 93.4 to 103.4%, and the RSD value ranged from 1.7 to 4.3%. It means that the novel ECL biosensor could be applied to detect real samples with good performance.

CONCLUSIONS

We have rationally designed a sensitive detection method for the SARS-CoV-2 RdRp gene based on a novel Au@Ti_3C_2@PEI-Ru(dcbpy)$_3^{2+}$ nanocomposite ECL biosensor with an unipedal DNA walker amplification strategy. Using Au@Ti_3C_2@PEI-Ru(dcbpy)$_3^{2+}$ nanocomposites can improve the sensitivity of the ECL biosensor, and it possessed the characteristics of excellent stability and outstanding luminescence performance. The Au NPs linked to DNA and Ru(dcbpy)$_3^{2+}$ with luminescent properties were fixed on the Ti_3C_2 surface to improve the sensitivity of the ECL biosensor. PEI can be interconnected with Ru(dcbpy)$_3^{2+}$ through an amide bond as a coreactant to improve the luminous efficiency of Ru(dcbpy)$_3^{2+}$. In particular, a unipedal DNA walker as an amplification strategy can effectively improve the sensitivity of the ECL biosensor. The unipedal DNA walker was activated by SARS-CoV-2 RdRp, resulting in the excision of HP DNAs bound to model DNA−AgNCs. Combining the unipedal DNA walker amplification strategy and constructing an ECL biosensor based on Au@Ti_3C_2@PEI-Ru(dcbpy)$_3^{2+}$ nanocomposites, more sensitive detection of the SARS-CoV-2 RdRp gene was achieved with an LOD of 0.21 fM. The novel ECL biosensor with reasonable specificity and stability would play an important role in early clinical diagnosis.

ASSOCIATED CONTENT

Supporting Information

The Supporting Information is available free of charge at https://pubs.acs.org/doi/10.1021/acsami.1c04453.

UV−vis absorption spectrum, ECL spectrum, HRTEM image, stability of nanocomposites, all sequences of oligonucleotides, comparison of different methods for SARS-CoV-2 detection, and recovery results for the assay of target DNA in human serum (PDF)

AUTHOR INFORMATION

Corresponding Authors

Jianfeng Zhao − *Key Laboratory of Flexible Electronics (KLOFE) & Institute of Advanced Materials (IAM), Jiangsu National Synergetic Innovation Center for Advanced Materials (SICAM), Nanjing Tech University (NanjingTech), Nanjing 211816, P.R. China*; Email: iamjfzhao@njtech.edu.cn

Kai Zhang − *NHC Key Laboratory of Nuclear Medicine, Jiangsu Key Laboratory of Molecular Nuclear Medicine, Jiangsu Institute of Nuclear Medicine, Wuxi, Jiangsu 214063, P.R. China*; orcid.org/0000-0002-7021-5395; Email: zhangkai@jsinm.org

Authors

Bo Yao − *Key Laboratory of Flexible Electronics (KLOFE) & Institute of Advanced Materials (IAM), Jiangsu National Synergetic Innovation Center for Advanced Materials (SICAM), Nanjing Tech University (NanjingTech), Nanjing 211816, P.R. China; NHC Key Laboratory of Nuclear Medicine, Jiangsu Key Laboratory of Molecular Nuclear Medicine, Jiangsu Institute of Nuclear Medicine, Wuxi, Jiangsu 214063, P.R. China*

Jing Zhang − *Key Laboratory of Flexible Electronics (KLOFE) & Institute of Advanced Materials (IAM), Jiangsu National Synergetic Innovation Center for Advanced Materials (SICAM), Nanjing Tech University (NanjingTech), Nanjing 211816, P.R. China*

Zhenqiang Fan − *NHC Key Laboratory of Nuclear Medicine, Jiangsu Key Laboratory of Molecular Nuclear Medicine, Jiangsu Institute of Nuclear Medicine, Wuxi, Jiangsu 214063, P.R. China*

Yuedi Ding − *NHC Key Laboratory of Nuclear Medicine, Jiangsu Key Laboratory of Molecular Nuclear Medicine,*

https://doi.org/10.1021/acsami.1c04453
ACS Appl. Mater. Interfaces 2021, 13, 19816−19824

Jiangsu Institute of Nuclear Medicine, Wuxi, Jiangsu 214063, P.R. China

Bin Zhou − *NHC Key Laboratory of Nuclear Medicine, Jiangsu Key Laboratory of Molecular Nuclear Medicine, Jiangsu Institute of Nuclear Medicine, Wuxi, Jiangsu 214063, P.R. China*

Runlin Yang − *NHC Key Laboratory of Nuclear Medicine, Jiangsu Key Laboratory of Molecular Nuclear Medicine, Jiangsu Institute of Nuclear Medicine, Wuxi, Jiangsu 214063, P.R. China*

Complete contact information is available at: https://pubs.acs.org/10.1021/acsami.1c04453

Author Contributions

[§]B.Y. and J.Z. contributed equally to this work.

Notes

The authors declare no competing financial interest.

■ ACKNOWLEDGMENTS

This work was supported by the National Natural Science Foundation of China (21705061), the Jiangsu Provincial Key Medical Discipline (Laboratory) (ZDXKA2016017), and the Innovation Capacity Development Plan of Jiangsu Province (BM2018023).

■ REFERENCES

(1) Liu, C.; Zhou, Q.; Li, Y.; Garner, L. V.; Watkins, S. P.; Carter, L. J.; Smoot, J.; Gregg, A. C.; Daniels, A. D.; Jervey, S.; Albaiu, D. Research and Development on Therapeutic Agents and Vaccines for COVID-19 and Related Human Coronavirus Diseases. *ACS Cent. Sci.* **2020**, *6*, 315−331.

(2) Ji, T.; Liu, Z.; Wang, G.; Guo, X.; Akbar khan, S.; Lai, C.; Chen, H.; Huang, S.; Xia, S.; Chen, B.; Jia, H.; Chen, Y.; Zhou, Q. Detection of COVID-19: A Review of the Current Literature and Future Perspectives. *Biosens. Bioelectron.* **2020**, *166*, 112455.

(3) Da Silva, S. J. R.; Silva, C. T. A. d.; Guarines, K. M.; Mendes, R. P. G.; Pardee, K.; Kohl, A.; Pena, L. Clinical and Laboratory Diagnosis of SARS-CoV-2, the Virus Causing COVID-19. *ACS Infect. Dis.* **2020**, *6*, 2319−2336.

(4) Udugama, B.; Kadhiresan, P.; Kozlowski, H. N.; Malekjahani, A.; Osborne, M.; Li, V. Y. C.; Chen, H.; Mubareka, S.; Gubbay, J. B.; Chan, W. C. W. Diagnosing COVID-19: The Disease and Tools for Detection. *ACS Nano* **2020**, *14*, 3822−3835.

(5) Karami, A.; Hasani, M.; Azizi Jalilian, F.; Ezati, R. Conventional PCR Assisted Single-Component Assembly of Spherical Nucleic Acids for Simple Colorimetric Detection of SARS-CoV-2. *Sens. Actuators, B* **2021**, *328*, 128971.

(6) Moitra, P.; Alafeef, M.; Dighe, K.; Frieman, M. B.; Pan, D. Selective Naked-Eye Detection of SARS-CoV-2 Mediated by N Gene Targeted Antisense Oligonucleotide Capped Plasmonic Nanoparticles. *ACS Nano* **2020**, *14*, 7617−7627.

(7) Zhou, P.; Yang, X.-L.; Wang, X.-G.; Hu, B.; Zhang, L.; Zhang, W.; Si, H.-R.; Zhu, Y.; Li, B.; Huang, C.-L.; Chen, H.-D.; Chen, J.; Luo, Y.; Guo, H.; Jiang, R.-D.; Liu, M.-Q.; Chen, Y.; Shen, X.-R.; Wang, X.; Zheng, X.-S.; Zhao, K.; Chen, Q.-J.; Deng, F.; Liu, L.-L.; Yan, B.; Zhan, F.-X.; Wang, Y.-Y.; Xiao, G.-F.; Shi, Z.-L. A Pneumonia Outbreak Associated with a New Coronavirus of Probable Bat Origin. *Nature* **2020**, *579*, 270−273.

(8) van Kasteren, P. B.; van der Veer, B.; van den Brink, S.; Wijsman, L.; de Jonge, J.; van den Brandt, A.; Molenkamp, R.; Reusken, C. B. E. M.; Meijer, A. Comparison of Seven Commercial RT-PCR Diagnostic Kits for COVID-19. *J. Clin. Virol.* **2020**, *128*, 104412.

(9) Tian, B.; Gao, F.; Fock, J.; Dufva, M.; Hansen, M. F. Homogeneous Circle-to-Circle Amplification for Real-Time Optomagnetic Detection of SARS-CoV-2 RdRp Coding Sequence. *Biosens. Bioelectron.* **2020**, *165*, 112356.

(10) Feng, W.; Newbigging, A. M.; Le, C.; Pang, B.; Peng, H.; Cao, Y.; Wu, J.; Abbas, G.; Song, J.; Wang, D.-B.; Cui, M.; Tao, J.; Tyrrell, D. L.; Zhang, X.-E.; Zhang, H.; Le, X. C. Molecular Diagnosis of COVID-19: Challenges and Research Needs. *Anal. Chem.* **2020**, *92*, 10196−10209.

(11) Reusken, C. B. E. M.; Broberg, E. K.; Haagmans, B.; Meijer, A.; Corman, V. M.; Papa, A.; Charrel, R.; Drosten, C.; Koopmans, M.; Leitmeyer, K. Behalf Of EVD-LabNet, On; ERLI-Net Laboratory Readiness and Response for Novel Coronavirus (2019-nCoV) in Expert Laboratories in 30 EU/EEA Countries, January 2020. *Eurosurveillance* **2020**, *25*, 2000082.

(12) Engelmann, I.; Alidjinou, E. K.; Ogiez, J.; Pagneux, Q.; Miloudi, S.; Benhalima, I.; Ouafi, M.; Sane, F.; Hober, D.; Roussel, A.; Cambillau, C.; Devos, D.; Boukherroub, R.; Szunerits, S. Preanalytical Issues and Cycle Threshold Values in SARS-CoV-2 Real-Time RT-PCR Testing: Should Test Results Include These? *ACS Omega* **2021**, *6*, 6528−6536.

(13) Corman, V. M.; Landt, O.; Kaiser, M.; Molenkamp, R.; Meijer, A.; Chu, D. K.; Bleicker, T.; Brunink, S.; Schneider, J.; Schmidt, M. L.; Mulders, D. G.; Haagmans, B. L.; van der Veer, B.; van den Brink, S.; Wijsman, L.; Goderski, G.; Romette, J. L.; Ellis, J.; Zambon, M.; Peiris, M.; Goossens, H.; Reusken, C.; Koopmans, M. P.; Drosten, C. Detection of 2019 Novel Coronavirus (2019-nCoV) by Real-Time RT-PCR. *Eurosurveillance* **2020**, *25*, 2000045.

(14) Fan, Z.; Lin, Z.; Wang, Z.; Wang, J.; Xie, M.; Zhao, J.; Zhang, K.; Huang, W. Dual-Wavelength Electrochemiluminescence Ratiometric Biosensor for NF-κB p50 Detection with Dimethylthiodiaminoterephthalate Fluorophore and Self-Assembled DNA Tetrahedron Nanostructures Probe. *ACS Appl. Mater. Interfaces* **2020**, *12*, 11409−11418.

(15) Liu, W.; Chen, A.; Li, S.; Peng, K.; Chai, Y.; Yuan, R. Perylene Derivative/Luminol Nanocomposite as a Strong Electrochemiluminescence Emitter for Construction of an Ultrasensitive MicroRNA Biosensor. *Anal. Chem.* **2019**, *91*, 1516−1523.

(16) Qi, H.; Li, M.; Dong, M.; Ruan, S.; Gao, Q.; Zhang, C. Electrogenerated Chemiluminescence Peptide-Based Biosensor for the Determination of Prostate-Specific Antigen Based on Target-Induced Cleavage of Peptide. *Anal. Chem.* **2014**, *86*, 1372−1379.

(17) Wu, F.-F.; Zhou, Y.; Zhang, H.; Yuan, R.; Chai, Y.-Q. Electrochemiluminescence Peptide-Based Biosensor with Hetero-Nanostructures as Coreaction Accelerator for the Ultrasensitive Determination of Tryptase. *Anal. Chem.* **2018**, *90*, 2263−2270.

(18) Zhang, K.; Fan, Z.; Yao, B.; Ding, Y.; Zhao, J.; Xie, M.; Pan, J. Exploring the Trans-Cleavage Activity of CRISPR-Cas12a for the Development of a Mxene Based Electrochemiluminescence Biosensor for the Detection of Siglec-5. *Biosens. Bioelectron.* **2021**, *178*, 113019.

(19) Fang, Y.; Yang, X.; Chen, T.; Xu, G.; Liu, M.; Liu, J.; Xu, Y. Two-Dimensional Titanium Carbide (MXene)-Based Solid-State Electrochemiluminescent Sensor for Label-Free Single-Nucleotide Mismatch Discrimination in Human Urine. *Sens. Actuators, B* **2018**, *263*, 400−407.

(20) Naguib, M.; Halim, J.; Lu, J.; Cook, K. M.; Hultman, L.; Gogotsi, Y.; Barsoum, M. W. New Two-Dimensional Niobium and Vanadium Carbides as Promising Materials for Li-Ion Batteries. *J. Am. Chem. Soc.* **2013**, *135*, 15966−15969.

(21) Zhang, H.; Wang, Z.; Wang, F.; Zhang, Y.; Wang, H.; Liu, Y. In Situ Formation of Gold Nanoparticles Decorated Ti_3C_2 MXenes Nanoprobe for Highly Sensitive Electrogenerated Chemiluminescence Detection of Exosomes and Their Surface Proteins. *Anal. Chem.* **2020**, *92*, 5546−5553.

(22) Zhang, H.; Wang, Z.; Zhang, Q.; Wang, F.; Liu, Y. Ti_3C_2 MXenes Nanosheets Catalyzed Highly Efficient Electrogenerated Chemiluminescence Biosensor for the Detection of Exosomes. *Biosens. Bioelectron.* **2019**, *124*−*125*, 184−190.

(23) Liu, J.-L.; Tang, Z.-L.; Zhang, J.-Q.; Chai, Y.-Q.; Zhuo, Y.; Yuan, R. Morphology-Controlled 9,10-Diphenylanthracene Nanoblocks as Electrochemiluminescence Emitters for MicroRNA Detection with One-Step DNA Walker Amplification. *Anal. Chem.* **2018**, *90*, 5298−5305.

(24) Mason, S. D.; Tang, Y.; Li, Y.; Xie, X.; Li, F. Emerging Bioanalytical Applications of DNA Walkers. *TrAC, Trends Anal. Chem.* **2018**, *107*, 212−221.
(25) Yang, X.; Tang, Y.; Mason, S. D.; Chen, J.; Li, F. Enzyme-Powered Three-Dimensional DNA Nanomachine for DNA Walking, Payload Release, and Biosensing. *ACS Nano* **2016**, *10*, 2324−2330.
(26) Chen, J.; Luo, Z.; Sun, C.; Huang, Z.; Zhou, C.; Yin, S.; Duan, Y.; Li, Y. Research Progress of DNA Walker and Its Recent Applications in Biosensor. *TrAC, Trends Anal. Chem.* **2019**, *120*, 115626.
(27) Yan, T.; Zhu, L.; Ju, H.; Lei, J. DNA-Walker-Induced Allosteric Switch for Tandem Signal Amplification with Palladium Nanoparticles/Metal−Organic Framework Tags in Electrochemical Biosensing. *Anal. Chem.* **2018**, *90*, 14493−14499.
(28) Huang, Y.; Zhu, X.; Jin, C.; Li, W.; Zhou, Y.; Yuan, R. Double-Site DNA Walker Based Ternary Electrochemiluminescent Biosensor. *Talanta* **2020**, *219*, 121274.
(29) Miao, P.; Tang, Y. Gold Nanoparticles-Based Multipedal DNA Walker for Ratiometric Detection of Circulating Tumor Cell. *Anal. Chem.* **2019**, *91*, 15187−15192.
(30) Zhang, L.; Xiong, C.; Wang, H.; Yuan, R.; Chai, Y. A Sensitive Electrochemiluminescence Immunosensor for Cardiac Troponin I Detection Based on Dual Quenching of the Self-Enhanced Ru(II) Complex by Folic Acid and in Situ Generated Oxygen. *Sens. Actuators, B* **2017**, *241*, 765−772.
(31) Zhang, Z.; Liu, T.; Yue, C.; Wang, S.; Ma, J.; Zhou, T.; Wang, F.; Wang, X.; Zhang, G. Label-Free and Ultrasensitive Fluorescence Assay for Fe^{3+} detection Using DNA-Templated Ag Nanoclusters. *Colloids Surf., A* **2019**, *579*, 123656.
(32) Liu, L.; Wei, Y.; Jiao, S.; Zhu, S.; Liu, X. A Novel Label-Free Strategy for the Ultrasensitive miRNA-182 Detection Based on MoS_2/Ti_3C_2 Nanohybrids. *Biosens. Bioelectron.* **2019**, *137*, 45−51.
(33) Hu, G.-B.; Xiong, C.-Y.; Liang, W.-B.; Zeng, X.-S.; Xu, H.-L.; Yang, Y.; Yao, L.-Y.; Yuan, R.; Xiao, D.-R. Highly Stable Mesoporous Luminescence-Functionalized MOF with Excellent Electrochemiluminescence Property for Ultrasensitive Immunosensor Construction. *ACS Appl. Mater. Interfaces* **2018**, *10*, 15913−15919.

https://doi.org/10.1021/acsami.1c04453
ACS Appl. Mater. Interfaces 2021, 13, 19816−19824